RESEARCH PAPER

Investigating the Mechanical Responses and Construction Optimization for Shallow Super-Large Span Tunnels in Weathered Tuff Stratum Based on Field Monitoring and Flac3D Modeling

Jiaxin He[1] · Shaohui He[1] · Xiabing Liu[2] · Jianfei Ma[1] · Yiming Li[1] · Bin Zhang[1]

Abstract

To investigate the mechanical responses and construction optimization of shallow super-large span (SLS) tunnels in weathered tuff stratum, the field monitoring scheme and the refined three-dimensional numerical model for Xiabeishan No.2 tunnel were established, and a sequence of field and laboratory tests was conducted to acquire the calculation parameters. Then, the surrounding rock pressure and shotcrete stress in grades III–V rock mass were comprehensively monitored and analyzed. Finally, according to the problems occurred in site construction, some optimized construction methods were proposed and then, systematically discussed by numerical simulation. The results show that: (1) it was discovered that the construction disturbance of the shallow SLS tunnel is mainly concentrated in the excavation of the upper benches; (2) the excavation of the upper bench of the middle heading, in which the super-large span structure is formed, is the most critical constructio n step; (3) the blasting vibration created by the excavation of middle heading caused serious damage to the temporary support, and the stress adjustment between the rock mass and supporting structures was completed before the demolition temporary support; (4) both the "middle first and side later" double side heading method in grades IV–V rock mass and the three-step method in grade III rock mass are feasible under certain conditions.

Keywords Shallow super-large span tunnels · Mechanical responses · Construction optimization · Field monitoring · Numerical simulation · Laboratory tests

✉ Shaohui He
  shhhe@bjtu.edu.cn

  Jiaxin He
  20115019@bjtu.edu.cn

  Xiabing Liu
  14115293@bjtu.edu.cn

  Jianfei Ma
  22110333@bjtu.edu.cn

  Yiming Li
  19115028@bjtu.edu.cn

  Bin Zhang
  18121053@bjtu.edu.cn

1   School of Civil Engineering, Beijing Jiaotong University, Beijing 100044, China

2   Guangdong Hualu Transport Technology Co., Ltd., Guangzhou 510420, China

1 Introduction

The super-large span (SLS) tunnels, with their spaciousness and higher traffic efficiency, have been widely adopted in highway traffic [1, 2], railway traffic [3, 4] and urban traffic [5, 6] in recent years. The sequential excavation method, which is the most frequently employed method in the excavation of SLS tunnels, can significantly reduce the construction risks. However, due to the large number of pilot tunnels and complicated construction steps of the sequential excavation method, the interactions between surrounding rock and supporting structures of SLS tunnels are extremely elusive [7–9].

Over the years, scholars have made a lot of achievements in the mechanical responses of surrounding rock and supporting structures of SLS tunnels. For example, based on a series of field tests, Li et al. [10] investigated the influence of the construction methods and support forms on the mechanical behaviors of primary support of SLS

tunnels in loess stratum. Luo et al. [11] and Qi et al. [12] obtained the stress distribution of the primary support of SLS tunnels through field monitoring. By utilizing the method of field tests and numerical simulation, Luo et al. [13] found that removing the temporary support and pouring the secondary lining significantly changed the internal force of the primary support of SLS tunnels. Zhou et al. [14] performed a field test to investigate the stress variation of the initial support of SLS tunnels under the double side heading method and found that the construction of the lower step of left heading and the upper step of middle heading were the key stages of load transfer between the rock mass and supporting structures. Tu et al. [6] paid special attention to the load-bearing characteristics of the composite lining of SLS tunnels and pointed out that the primary support was the major load-bearing structure, and the secondary lining mainly plays the role of safety reserve. Based on field monitoring, Chen et al. [15, 16] analyzed the internal forces of the surrounding rock, steel frame, shotcrete and rock bolts of SLS tunnels. It was revealed that the steel frame and surrounding rock were the major load-bearing structures, while the shotcrete and systematic bolts played an auxiliary supporting role.

The tunnel spans in the research mentioned above, however, are around 20 m. At present, there are very few engineering cases in which the tunnel span exceeds 25m. Based on model experiments and numerical simulations, Liu et al. [17] revealed the evolution and distribution of the ground stress of Hongqihegou station (the span is 25.6 m). Wu [18] obtained the development of the stratum deformation of Wulidian Station (the span is 27.1 m) through field monitoring. Taking the exit section of the Wufengshan No. 2 tunnel (the span is 28.4 m) as the research background, Qing et al. [19] and Zhao et al. [8] investigated the mechanical responses of the surrounding rock under different construction methods. Hong and Zhang [20] investigated the stress characteristics of the composite lining in the exit section of Xinaotang tunnel (the span is 30.3 m) by numerical simulation, but their research lacked verification of the monitoring data. In general, the majority of current research on SLS tunnels with spans over 25 m focuses on the stress and deformation of surrounding rock, with little attention paid to the mechanical behavior of support structures.

Therefore, this paper takes the Xiabeishan No.2 tunnel project of Hangzhou–Shaoxing–Taizhou high-speed railway as the background. Firstly, the field monitoring scheme and the refined three-dimensional numerical model for Xiabeishan No.2 tunnel were established, and a sequence of field and laboratory tests was conducted to acquire the calculation parameters. Then, the surrounding rock pressure and shotcrete stress of the shallow SLS tunnel in grades III–V rock mass were comprehensively monitored and analyzed. Finally, according to the problems occurred in site construction, some optimized construction methods were proposed and then, systematically discussed by numerical simulation. The research achievement might provide beneficial reference for similar projects.

2 Engineering Overview

2.1 Site Conditions

As shown in Fig. 1, the Hangzhou–Shaoxing–Taizhou high-speed railway connects Hangzhou city, Shaoxing city and Taizhou city in China. The Xiabeishan No. 2 tunnel, which is located in Taizhou City, is the crucial project of Hangzhou–Shaoxing–Taizhou high-speed railway. The tunnel is designed as a four-line shallow super-large span (SLS) tunnel since it is close to the railway station of Taizhou. The length and maximum buried depth of Xiabeishan No.2 tunnel are 430 m and 57 m, respectively. The excavation span of the tunnel is 26.3 m, the maximum excavation span of the widened section is 27.3m, and the maximum excavation area is 361 m^2.

As shown in Fig. 2, the surface of the Xiabeishan mountain is covered with 2–4 m thick silty clay, and the inside is weathered tuff. The tuff stratum at the entrance of the tunnel has been strongly weathered, and the rock joints are extremely developed. The diameter of the rock blocks is about 2cm to 30cm, and clay layers with thicknesses of 1cm to 5cm are formed in local areas. Along the tunnel entrance, the weathering degree of the surrounding rock gradually decreases. Based on the BQ rock classification system of, the entrance and exit section of the Xiabeishan No. 2 tunnel is grade V rock mass, and the tunnel body are grades III–IV rock mass.

2.2 Support Parameters and Excavation Method

At present, the double side heading method is generally adopted in the construction of SLS tunnels, such as the Wulidian Station [18], Wufengshan No. 2 tunnel [19] and Xinkaotang tunnel [20] and Fenghuangshan tunnel [21]. Based on these engineering experiences, the double side heading method, with the excavation sequence from the side heading to the middle heading, is adopted for the construction of Xiabeishan No. 2 tunnel (as shown in Fig. 3). The drifts are excavated by drilling and blasting, and the staggered distance of adjacent drift is 10–20m. The excavation footage of grades III–V rock mass is 1.2 m, 1 m and 0.8 m, respectively. The supporting parameter ades III–V rock mass are listed in Table 1.
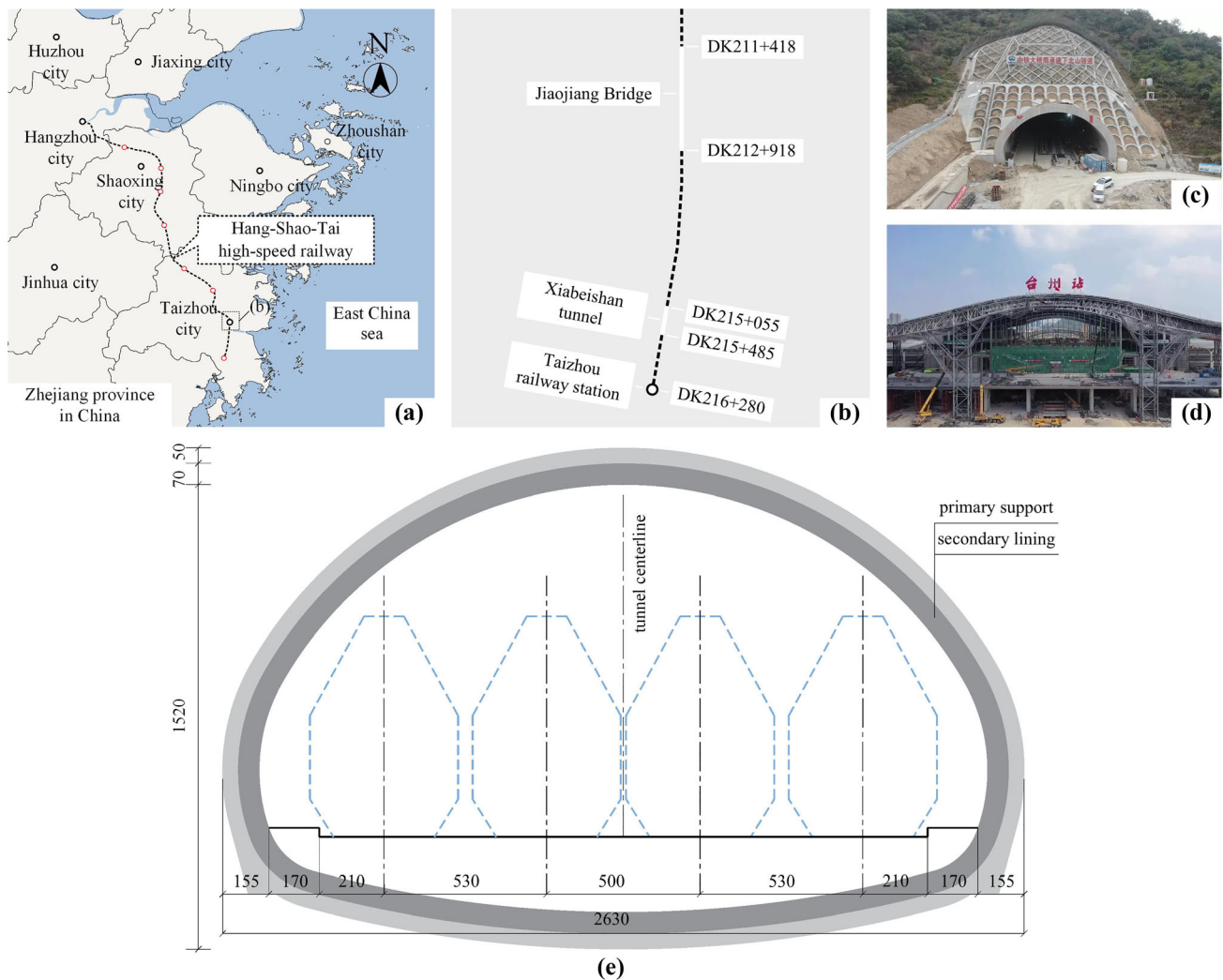
Fig. 1 Project overview (unit: cm): **a** project location, **b** tunnel surroundings, **c** Xiabeishan No.2 tunnel, **d** Taizhou Railway Station, **e** tunnel cross section

3 Methods

3.1 Field Monitoring

Three sections with mileages of DK215 + 127 (Sect. 1), DK215 + 181 (Sect. 2) and DK215 + 202 (Sect. 3) were chosen for field monitoring. The grades of the rock mass in Sects. 1, 2, 3 are V, IV and III, respectively. As shown in Fig. 4, in each section, fourteen internal force measuring points were arranged: vault (point A), arch shoulder (points B and N), arch waist (points C and M), arch foot (points D and L), wall waist (points E and K), wall foot (points F and J), left and right invert (points G and I), and middle invert (point H). As displayed in Fig. 5, the double-membrane pressure cells were closely attached to surrounding rock and fixed by steel bracket to monitor the surrounding rock pressure; the concrete strain gauges were symmetrically

fixed on the two edges of the shotcrete to monitor the shotcrete stress.

The measured values were collected manually for the period from March 2019 to April 2021. According to the technical specification [22], the measured values were collected once per day in the initial stage, and then, the collection frequency gradually reduced. Some monitoring sensors, especially concrete strain gauges, were accidentally damaged during construction, and no data were obtained (Fig. 10).

3.2 Numerical Simulation

In the simulation of tunnel construction, the finite element difference method shows great advantages, such as high calculation accuracy, high flexibility in grid density and difference formula selection, and easy realization and visualization [23–25]. Therefore, the FLAC 3D, a
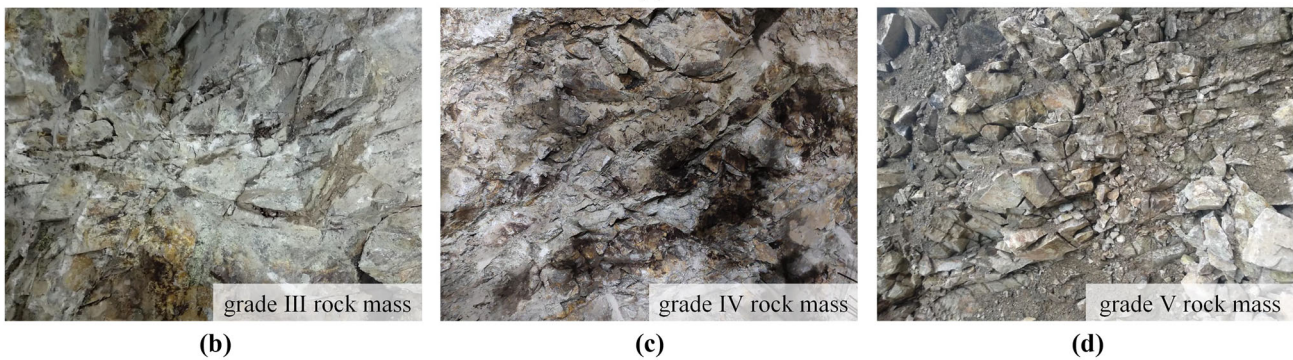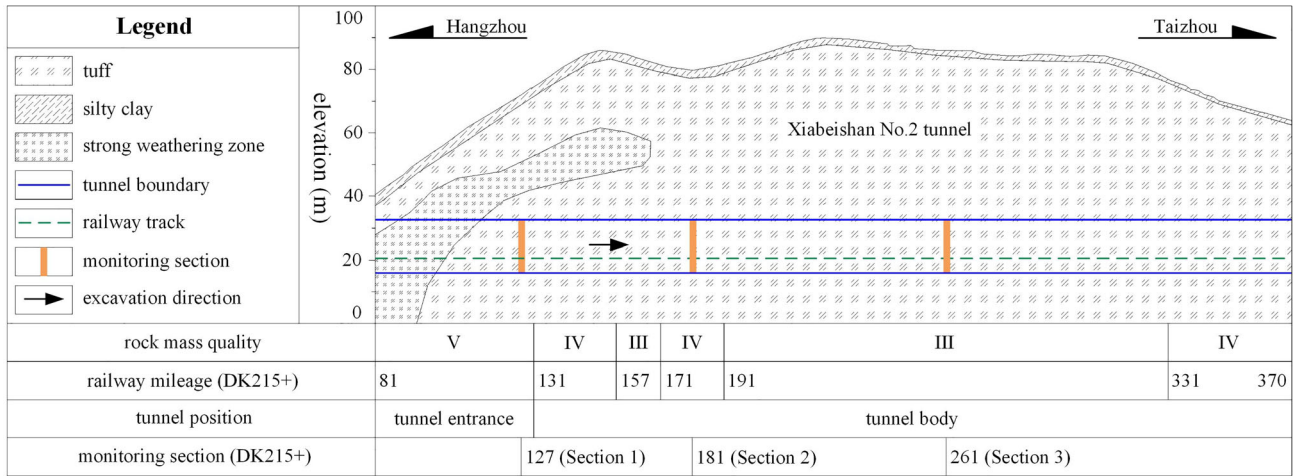
Fig. 2 Geological conditions: **a** longitudinal section, **b** grade III rock mass, **c** grade IV rock mass, **d** grade V rock mass
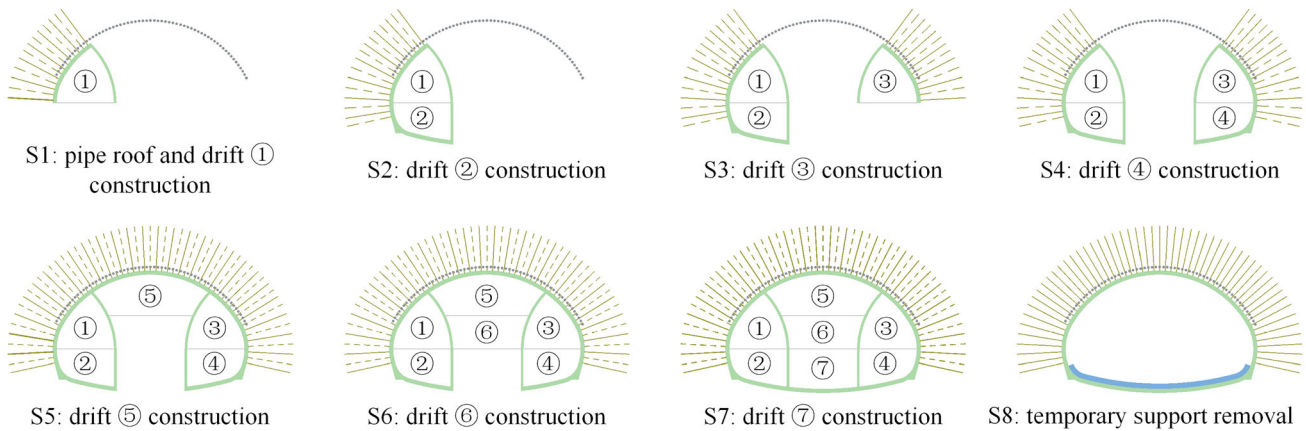

Fig. 3 Construction sequence of Xiabeishan No. 2 tunnel

representative commercial calculation software using finite difference method, was adopted.

As shown in Fig. 6, the numerical calculation flow mainly includes establishing geometric model, setting boundary conditions, determining calculation parameters, selecting constitutive model and yield criterion, initial

geostress balance and cyclic excavation. According to Fenner's solution [26], the tunnel construction has little effect on the surrounding rock beyond 5 times the radius of the tunnel. To eliminate the boundary effect, the length from the tunnel boundary to the model boundary is set to 5 times the tunnel radius, and the total width, length and

Table 1 Supporting parameters of the Xiabeishan No. 2 tunnel

Support Type	Grade III rock mass	Grade IV rock mass	Grade V rock mass
Primary support			
C30 shotcrete	Thickness: 35 cm	Thickness: 45 cm	Thickness: 50 cm
Steel arch	I18; spacing: 1.2 m	I20b; spacing: 1.0 m	I22b; spacing: 0.8 m
ϕ 32 mm systematic bolts	Length: 5m; spacing: 2.0×1.2 m	Length: 6m; spacing: 1.5×1.0 m	Length: 6m; spacing: 1.5×0.8 m
	Position: arch and side wall	Position: arch and side wall	Position: arch and side wall
Temporary support			
C30 shotcrete	Thickness: 25 cm	Thickness: 25 cm	Thickness: 25 cm
Steel arch	I18; spacing: 1.2 m	I20b; spacing: 1.0 m	I22b; spacing: 0.8 m
Secondary lining			
C30 shotcrete	Thickness: 60 cm	Thickness: 70 cm	Thickness: 70 cm
Reinforcement	ϕ 22 mm	ϕ 22 mm	ϕ 25 mm
	Spacing: 20×20 cm	Spacing: 20×20 cm	Spacing: 20×20 cm
Auxiliary support structure			
Pipe shed	–	–	ϕ 159 mm pipe shed
ϕ 50 mm locking anchor pipe	Length: 5 m; thickness: 4 mm; position: arch shoulder, arch foot, wall waist and wall foot		

height of the model of Xiabeishan No.2 tunnel, including the topography, are 156 m, 120 m and 90–140 m, respectively (as shown in Fig. 7). Vitali et al. [27] pointed out that when the grid size of surrounding rock near the tunnel is less than 0.1 times the tunnel span, the numerical calculation error is within the acceptable range. Therefore, in this numerical simulation, the grid size of surrounding rock near the tunnel is 1m (the span of each heading is about 10m). With the increase in distance from the tunnel, the grid size of surrounding rock gradually increases, and the grid size at the model boundary is 4–6m.

Fixed constraints and normal constraints are set at the model bottom and model sides, respectively, and model top is set as a free surface. The surrounding rock is simulated by homogeneous hexahedral elements and followed the Mohr–Coulomb criterion, and the acquisition of mechanical parameters of surrounding rock can be seen in Sect. 3.3. The secondary lining and temporary support are simulated by homogeneous hexahedral elements with linear elasticity. The primary support is simulated by shell elements. The steel arches in the supporting structures are converted to concrete relying on their elastic modulus and cross-sectional area. The calculation parameters of these supporting structures are listed in Table 2.

The pipe shed and systematic bolts are simulated by cable elements and beam elements, respectively. The mechanical parameters of bolts are determined by a series of simulated bolt tests and listed in Table 3. The calculation parameters of pipe shed are calculated according to its geometric size and listed in Table 4. The excavation sequence, excavation footage, lagging distance of adjacent drifts, and other calculation parameters are consistent with

Sect. 2.2. For the principle of finite difference method, as well as the yield equation and the plastic potential equation of surrounding rock, see the research of Xiao et al. [28], Lee et al. [29] and He et al. [30].

3.3 Field and Laboratory Tests

As shown in Fig. 8, the calculation parameters of the weathered tuff in Xiabeishan No.2 tunnel are derived by field investigation, laboratory tests, and geological investigation. Firstly, the tuff samples of Group A (grades III–VI rock mass) and Group B (grade V rock mass) with different weathering degrees were obtained through the core-drilling sampling at the tunnel site area. Then, based on the standard [31], the cylindrical standard specimens, with a diameter of 50 mm and a height of 100 mm, are manufactured. Later, a sequence of laboratory tests including the uniaxial compression test, triaxial compression test, and splitting test were conducted to collect the mechanical parameters of tuff samples. The Hoek–Brown nonlinear strength criterion has been employed to fit the laboratory test results, and the material constant, uniaxial compressive strength, uniaxial tensile strength, and average elastic modulus of group A samples are 16.9, 60.9 MPa, -3.59 MPa, and 23.4GPa, respectively, while those of group B are 10.8, 25.8 MPa, -2.36 MPa, and 15.1GPa, respectively. Besides, the GSI of grades III–V tuff stratum are determined as 44, 26, and 12 through the on-site geological investigation. Finally, based on the fitting method of equivalent Mohr–Coulomb strength parameters [32–34], the calculation parameters of grades III–V tuff stratum are calculated and listed in Table 5.
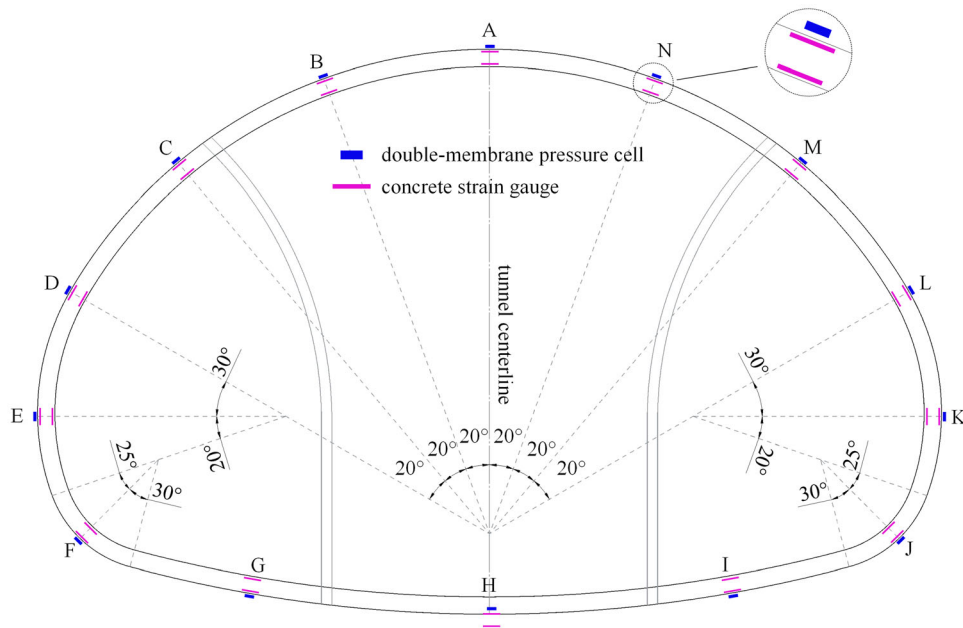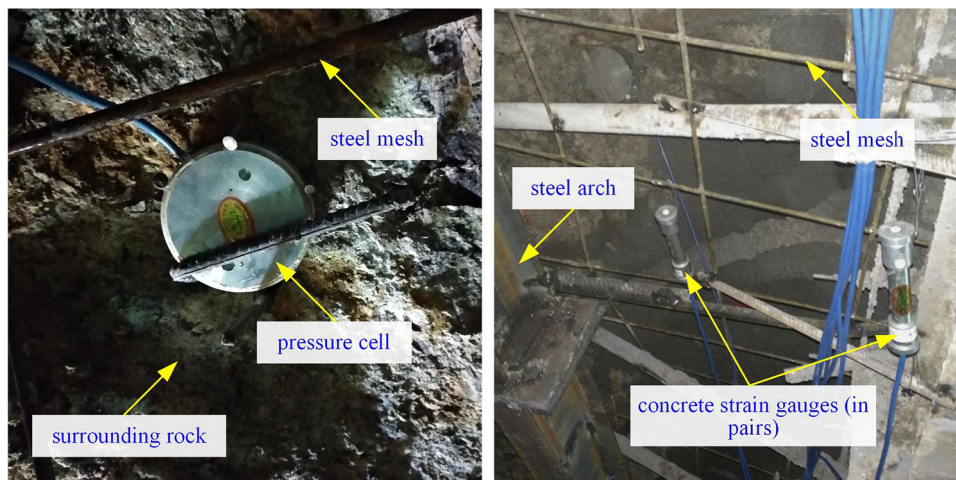
Fig. 4 Measuring points arrangement

Fig. 5 Installation of monitoring sensors

4 Monitoring Results and Analysis

4.1 Surrounding Rock Pressure

In view of the symmetry of the tunnel shape and excavation blocks, the measured values of symmetrical measuring points are relatively close. For convenience, this paper only analyzes the monitoring values on the left side of the tunnel (i.e., points A–F). S1–S8 represent various construction stages, respectively, and the specific meanings are shown in Fig. 3. Positive values indicate pressure and negative values represent tension.

The dynamic evolution of the surrounding rock pressure of Sects. 1, 2, 3 is displayed in Fig. 9. The pressure

development of the three sections showed the same characteristics. The rock pressure jumped noticeably after the construction of the upper benches of the three headings (i.e., Step S1, S3 and S5), and the pressure increment in the first two weeks after the excavation reached 60–90% of the final pressure. The main reason for the phenomenon is that the stress adjustment of the surrounding rock is concentrated on the early stage after excavation. Relatively, the pressure increment produced by the construction of the lower benches (i.e., Step S2, S4 and S5–S6) is far less than the former. This discovery indicates that the disturbance created by the construction of SLS tunnel is mainly concentrated in the construction of the upper benches, and the impact of the lower bench construction is very small. After
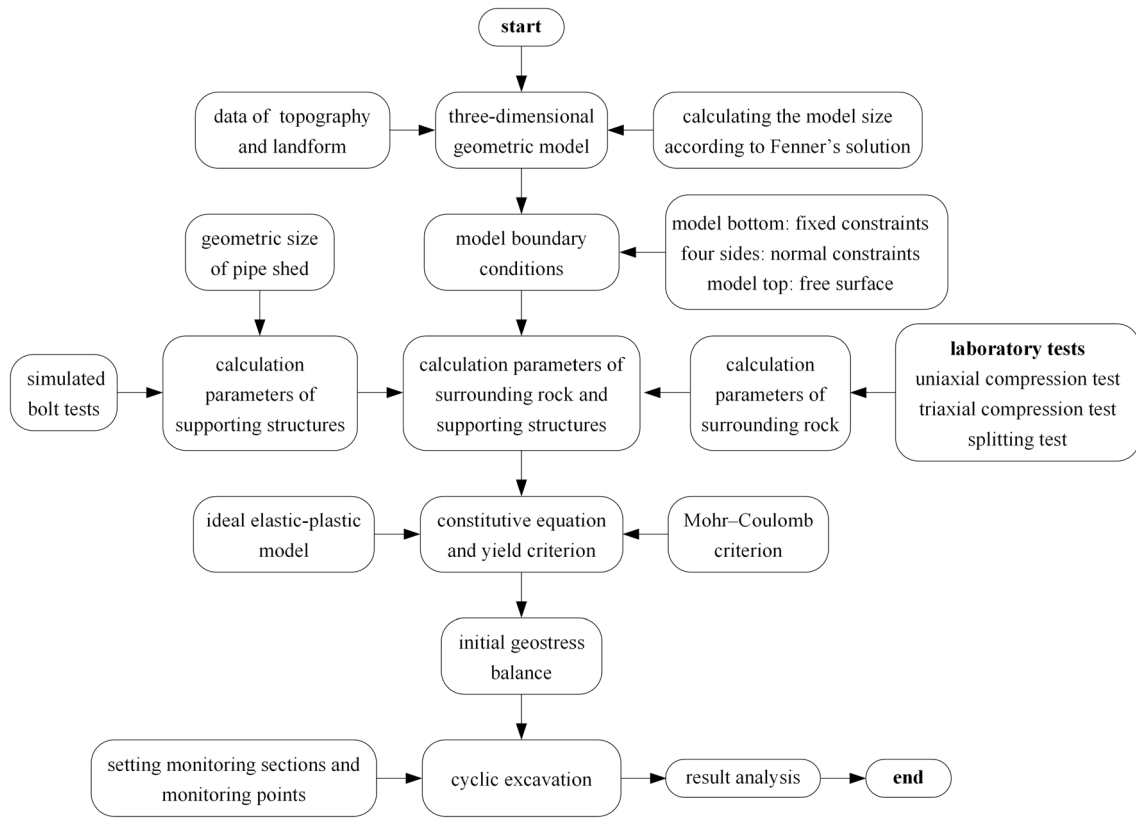
Fig. 6 The flowchart of the numerical simulation
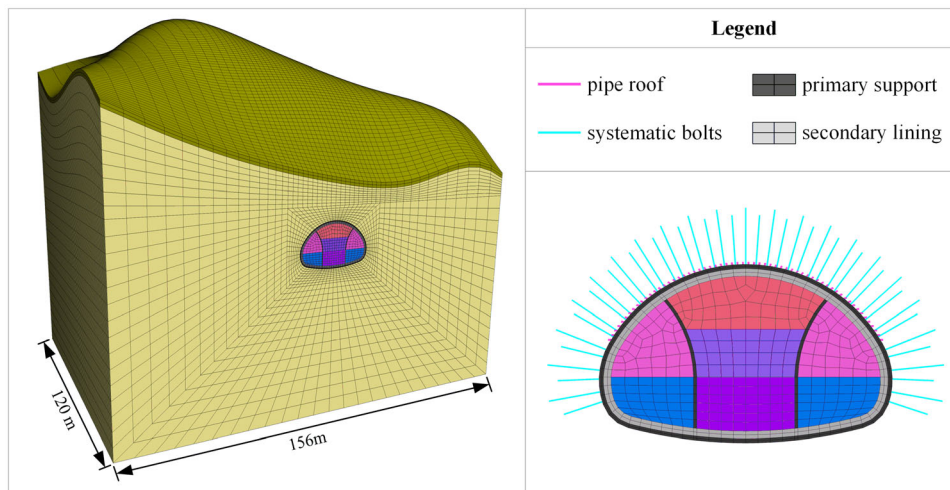

Fig. 7 Numerical model

the construction of the middle and lower benches of the middle heading (S6–S7), the primary support developed a closed-loop structure, and the rock pressure gradually stabilized over time.

The support removal effect refers to the phenomenon that the lining stress and the rock pressure change rapidly due to the removal of temporary supports, and the support removal effect is often more significant in the construction of SLS tunnels due to the large span, which causes great construction risks [35–38]. In the Xiabeishan No.2 tunnel project, the surrounding rock pressure increased by 10–20% during the excavation of the middle and lower benches of the middle heading (i.e., Step S6–S7), while surrounding rock pressure remained almost unchanged in the temporary support removal stage (i.e., Step S8). These phenomena can be attributed to the fact that the blasting

Table 2 Calculation parameters of the support structures

Type	Thickness (m)	Gravity density (kn·m^{-3})	Elastic modulus (gpa)	Poisson's ratio
Primary support	0.5	25	27.33	0.2
Temporary support	0.25	25	29.65	0.2
Secondary lining	0.7	25	34.9	0.2

Table 3 Calculation parameters of the systematic bolts

Ground condition	Bolts	Grout-Stiffness (kN·m^{-2})	Grout-cohesion (MPa)	Grout-friction (°)
Grade III rock mass	Anchor head	5×10^7	550	50
	Anchorage section	5×10^6	55	30
Grade IV rock mass	Anchor head	2.6×10^7	300	50
	Anchorage section	2.6×10^6	30	30
Grade V rock mass	Anchor head	1.05×10^7	200	50
	Anchorage section	1.05×10^6	20	30

The cross-sectional area of bolts is 3.52×10^{-4} m^2, the elastic modulus is 200 GPa, and the grouting perimeter is 0.314 m

vibration created by the construction of the middle heading caused serious damage to the temporary support, and the support removal effect was completed before the demolition of the temporary support. Therefore, to reduce the construction risk, the accuracy of drilling and charging should be strictly guaranteed, and the lining thickness and reinforcement ratio of the temporary support should be appropriately increased in the construction of the shallow SLS tunnels.

The sable distribution of the rock pressure is displayed in Fig. 10. The rock pressure of the three sections is mainly concentrated in tunnel arch, while the rock pressure at side wall and inverted arch is relatively small, showing a distribution pattern of "large in upper bench, small in lower

bench." This distribution pattern could be attributed to the small buried depth and super-large span of the tunnel, and the vertical stress in the ground stress field is greater than the horizontal stress. The average rock pressure of Sect. 1 is 71.8 kPa, which is about 2.2 times that of Sect. 3 (33.2 kPa). This result indicates that the rock pressure of shallow SLS tunnel is significantly affected by the rock conditions. Therefore, effective measures such as applying the pipe shed, increasing the shotcrete thickness, improving the strength grade and distribution density of the steel arch, and shortening the spacing of the rock bolts were adopted in subsequent construction.

4.2 Internal Force in Shotcrete

Assuming that shotcrete is uniform and continuous, and the shotcrete stress is linearly distributed. Therefore, the circumferential stress σ and bending moment M of the shotcrete can be obtained by Eqs. (1) and (2), respectively [39].

$$\sigma = \frac{1}{2}(\sigma_{inner} + \sigma_{outer}) \tag{1}$$

$$M = \frac{1}{2}(\sigma_{outer} - \sigma_{inner})W \tag{2}$$

where σ_{inner} and σ_{outer} represent the stress measured in the two edges of the shotcrete; W is the bending modulus and $W = bh^2/6$; b and h are the unit tunnel length and shotcrete thickness, respectively.

The development of the shotcrete stress is plotted in Fig. 11. Similar to the development of rock pressure, the shotcrete stress increased dramatically in the first two weeks after the construction of the upper benches of the three headings (i.e., Step S1, S3 and S5). The construction of the upper bench of the middle heading (i.e., Step S5) is the most critical construction step. During this period, the stress increment of shotcrete in the middle heading reached 65–90% of the final stress, and the shotcrete stress in the two side headings increased by 30–40%. However, under the excavation of the lagging right heading, the shotcrete stress in the leading left heading remained almost constant, which indicates that the excavation of the middle heading significantly affects the shotcrete stress of the side headings, but the interaction between the two side headings is very weak. During the excavation of the middle and lower

Table 4 Calculation parameters of the pipe shed

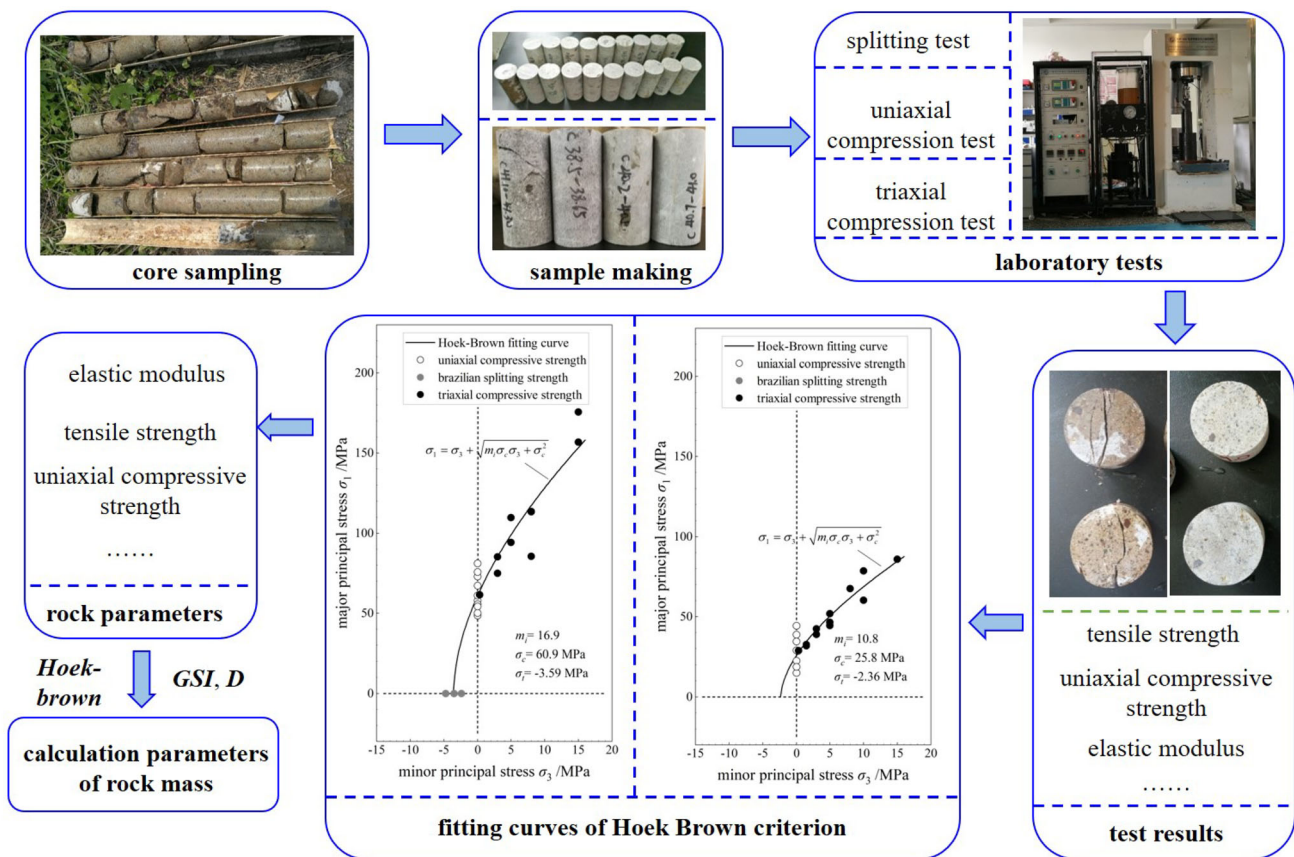| Type	Area (m^2)	Gravity density (kN·m^{-3})	Elastic modulus (GPa)	Inertia moment-z (m^4)	Inertia moment-x (m^4)	Poisson's ratio
Pipe shed	4.68×10^{-3}	78.5	200	1.33×10^{-5}	1.33×10^{-5}	0.27

Fig. 8 Process of obtaining the mechanical parameters of rock mass

Table 5 Calculation parameters of weathered tuff of Xiabeishan No.2 tunnel

Type	Thickness (m)	Gravity density (kN·m^{-3})	Elastic modulus (GPa)	Poisson's ratio	Cohesion (kPa)	Internal friction angle (°)
Silty clay	2	18.5	0.07	0.4	31	28.5
Grade V tuff	103.4	20	0.35	0.33	254	9.1
Grade IV tuff	111.2	22	0.73	0.30	1372	16.9
Grade III tuff	117.4	23	1.72	0.26	2232	24.3

benches of middle heading (i.e., Step S6–S7), the shotcrete stress in the three sections all increased by 10–20%, while the shotcrete stress changed little (about 5%) in the temporary support removal stage (i.e., Step S8). These development trends were in good agreement with the evolutionary pattern of the rock pressure, which once again shows that the support removal effect is completed before the demolition of the temporary support.

The stable distribution of the shotcrete stress and bending moment is demonstrated in Fig. 12. The shotcrete is predominantly subjected to compressive stress, and the distribution of the shotcrete stress in the three monitoring sections is relatively similar. Different from the distribution pattern of rock pressure, the shotcrete stress is mainly concentrated in the side walls, while the shotcrete stress in the tunnel arch and inverted arch is relatively small, showing a distribution mode of "large in side wall, small in arch and inverted arch." The average shotcrete stress in Sect. 1 is 8.24 MPa, which is significantly larger than that in Sect. 2 (6.68 MPa) and Sect. 3 (4.16 MPa). Based on the circumferential stress and the cross-sectional area, the axial force of shotcrete is determined. Thus, the average axial force of the shotcrete in Sects. 1, 2, 3 is 4121 kN, 2776 kN and 1536 kN, respectively. The axial force of shotcrete in Sect. 1 is about 2.7 times that of Sect. 3, which once again shows that the surrounding rock conditions significantly affect the stress of the supporting structure of shallow SLS tunnels.
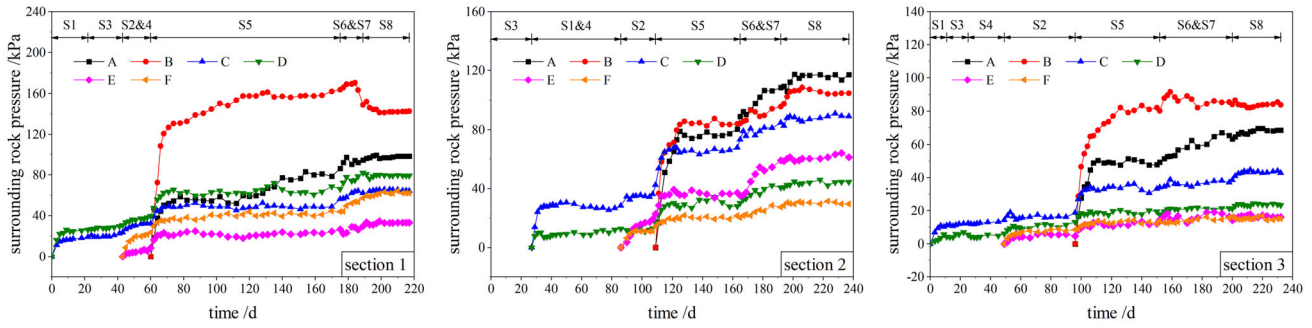
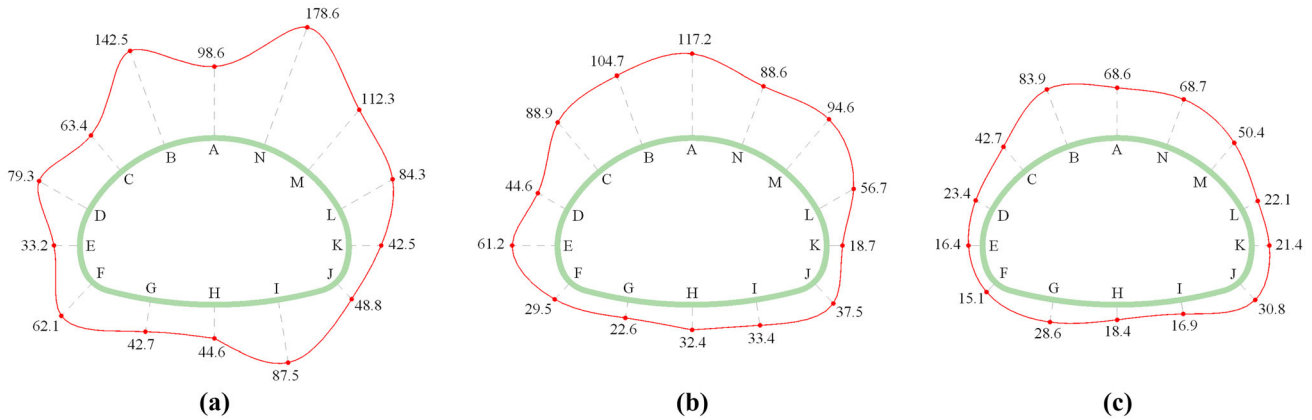Fig. 9 Development of the surrounding rock pressure

Fig. 10 Stable distribution of the surrounding rock pressure (unit: kPa): (a) section 1 (grade V rock mass), (b) section 2 (grade IV rock mass), (c) section 3 (grade III rock mass)
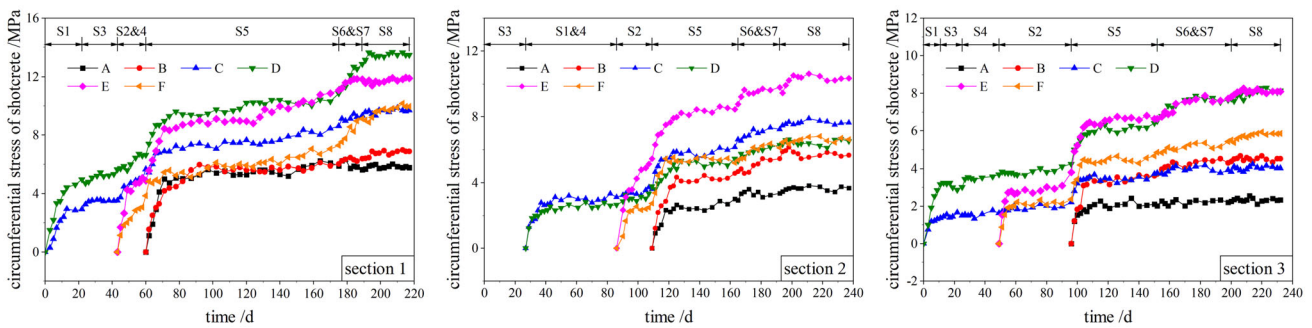

Fig. 11 Development of the shotcrete stress

Due to the inherent properties of the concrete, not only the compressive failure but also the bending failure of the shotcrete should be considered in tunnel construction. Because of the large excavation section and insufficient number of measuring points, only the approximate distribution of the bending moment of shotcrete was obtained. As shown in Fig. 12d–f, the largest positive bending moment is located at the vault (i.e., point A), while the largest negative bending moment is located at the arch shoulder (i.e., points B or N). Therefore, locking anchor pipes in these positions were accordingly applied, and the

observation of shotcrete deformation was strengthened in subsequent tunnel construction.

The safety factor that based on strength is the key parameter to quantitatively assess the safety of shotcrete. According to the standard [40], the calculation of the safety factor is as follows.

$$K \leq \varphi \alpha R_c / \sigma \qquad (e_0 \leq 0.2h) \qquad (3)$$

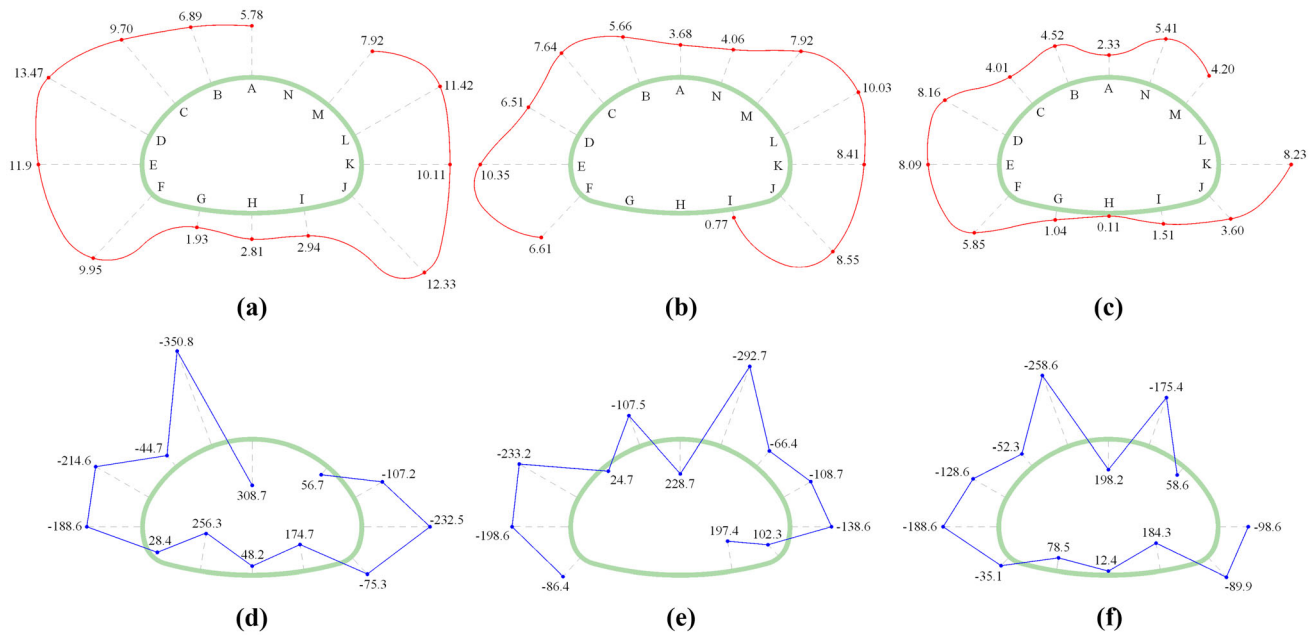$$K \leq \varphi \frac{1.75 R_t}{\sigma(6e_0/h - 1)} \qquad (e_0 > 0.2h) \qquad (4)$$

Fig. 12 Stable distribution of the circumferential stress (unit: MPa) and bending moment (unit: kN·m) in shotcrete: **a** stress at Sect. 1, **b** stress at Sect. 2, **c** stress at Sect. 3, **d** bending moment at Sect. 1, **e** bending moment at Sect. 2, **f** bending moment at Sect. 3

Table 6 Minimum safety factor of shotcrete

Sections	Minimum safety factor (compressive strength control)		Minimum safety factor (tensile strength control)	
	Value	Position	Value	Position
Section 1	1.63	Left arch foot (D)	4.12	Left invert (G)
Section 2	2.13	Left wall waist (E)	1.87	Right invert (I)
Section 3	2.67	Right wall waist (K)	2.79	Right invert (I)

where R_t and R_c represent the ultimate tensile strength and ultimate compressive strength of concrete and are taken as 2.2 MPa and 22 MPa, respectively; φ and α are calculation parameters. When $e_0 \leq 0.20h$, the bearing capacity of the shotcrete is determined by compressive strength, and Eq. (3) is used; otherwise, the concrete is controlled by tensile strength and Eq. (4) should be adopted. As displayed in Table 6, the minimum safety factor of Sect. 1 is 1.63 (located at D), considerably smaller than that of Sect. 2 (1.87 at E) and Sect. 3 (2.67 at K). All safety factors are greater than 1.0, indicating that the shotcrete is safe during tunnel construction.

5 Construction Optimization for Shallow SLS Tunnels

The safety evaluation results of the shotcrete showed that the site construction method ("side first and middle later" double side heading method) can meet the safety

requirements, and the Xiabeishan No. 2 tunnel was completed safely in April 2021. However, the following problems still exist in site construction:

1) It is difficult to accurately locate the reserved steel arches in the two side headings, resulting in the inaccurate and unstable connection between reserved steel arches and the steel arches of the middle heading, which caused great construction risks.
2) The tunnel length in grade III rock mass exceeded 50% of the total length, and the primary support of this section has a high safety margin. A large number of pilot tunnels and complicated construction steps increased the construction cost and delayed the construction period.

Therefore, the construction of the Xiabeishan No. 2 tunnel still needs optimization. For grades IV–V rock mass, the connection problem of the steel arches could be directly solved by excavating the middle heading first. Therefore, the site construction method can be changed to the "middle first and side later" double side heading method, such as the methods 1–3 in Fig. 13. For grade III rock mass, the three-step method can be considered (such as methods 4–6) to simplify the construction steps and reduce the construction cost. It is worth mentioning that the three-step method has been successfully applied in Wufengshan No.2 Tunnel [19, 41] and Badaling Great Wall Station [42].
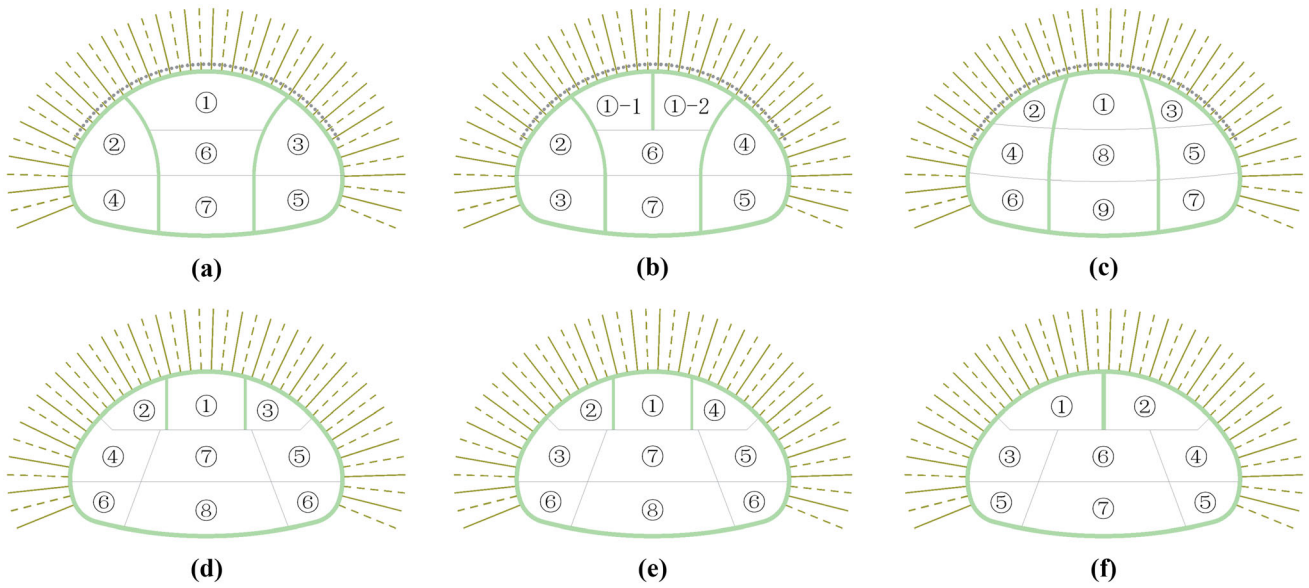
Fig. 13 Six o optimized construction schemes: **a** method 1, **b** method 2, **c** method 3, **d** method 4, **e** method 5, **f** method 6

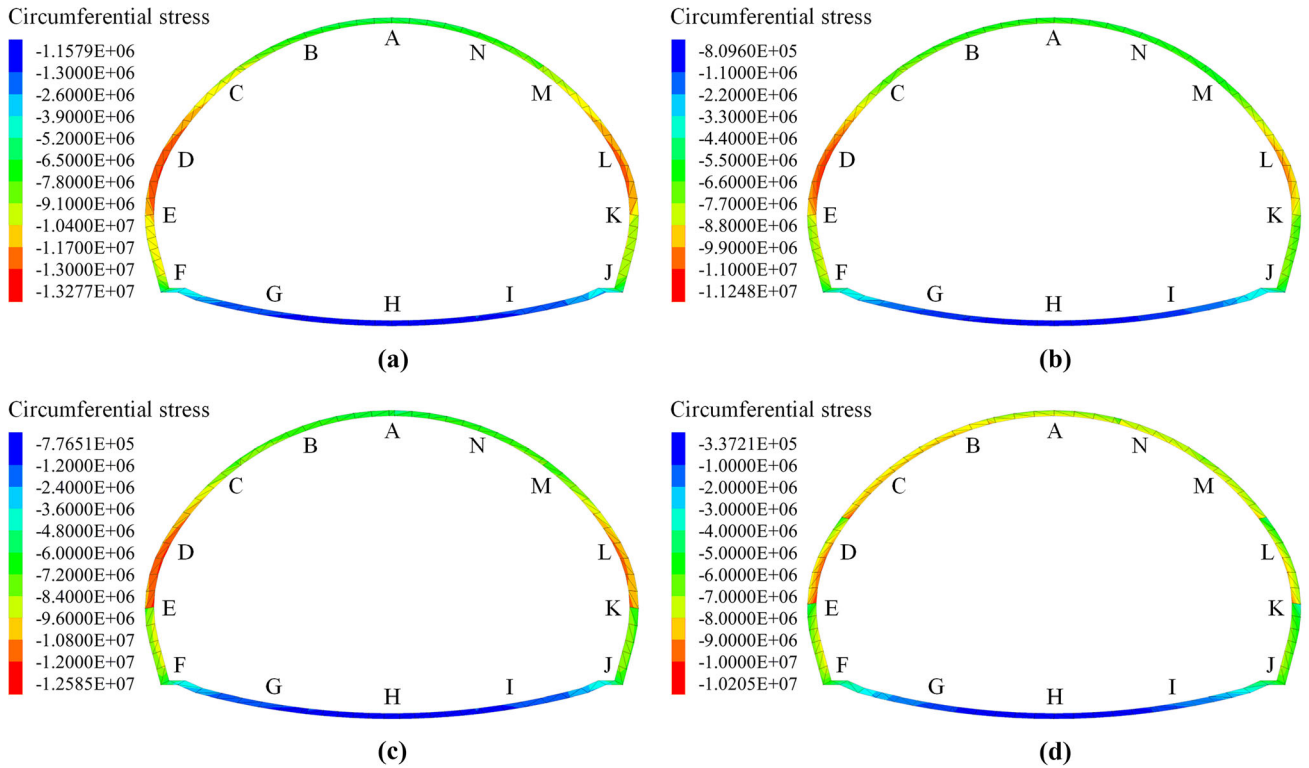Fig. 14 Lining stress distribution of the site construction method and method 1–3 in grade V rock mass (unit: Pa): **a** site construction method, **b** method 1, **c** method 2, **d** method 3
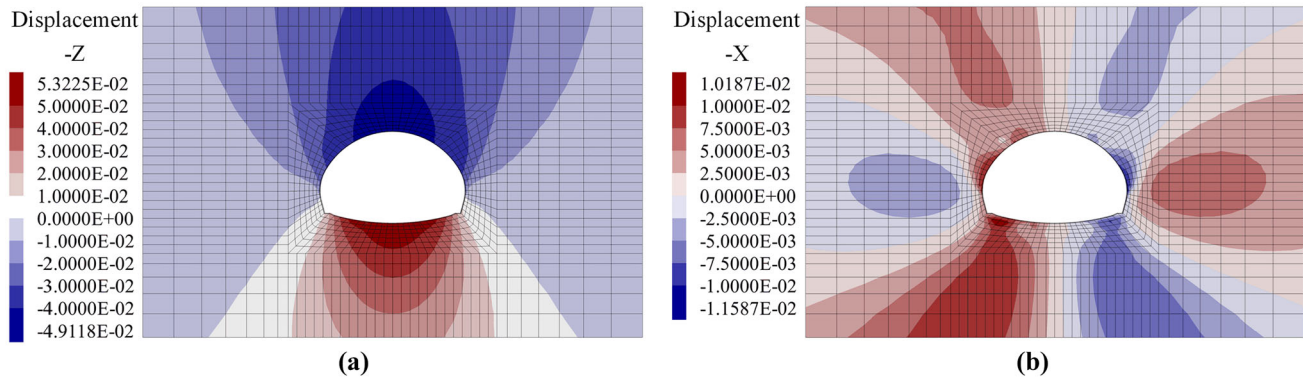
Fig. 15 Rock displacement distribution of the site construction method in grade V rock mass (unit: m): **a** vertical settlement, **b** horizontal convergence

6 Numerical Results and Analysis

6.1 Construction Optimization in Grade V Rock Mass

In grade V rock mass, the circumferential stress distribution of the primary support under the site construction method and methods 1–3 is illustrated in Fig. 14. The stress distributions of the four methods are relatively similar. The shotcrete stress in side wall is significantly larger than that in tunnel arch and inverted arch, which is in good agreement with monitoring results. The largest lining stress of the site construction method is 13.28 MPa, which is significantly larger than that of method 1 (11.25 MPa), method 2 (12.59 MPa) and method 3 (10.21 MPa). This result indicates that compared with the site construction method, the three optimization methods are more conducive to the safety of the primary support of shallow SLS tunnel.

The distribution of rock displacement of the site construction method in grade V rock mass is exhibited in Fig. 15. The rock displacement of methods 1–3 is not exhibited since they are close to those of the site construction method. The vertical displacement is concentrated in tunnel arch and inverted arch, while the horizontal displacement is predominantly distributed in side wall. The maximum vault settlements of methods 1–3 are 70.3 mm, 63.2 mm and 82.8 mm, and the largest horizontal convergence are 66.6 mm, 50.6 mm and 60.9 mm, respectively, all of which are larger than the maximum vault settlement (49.1mm) and horizontal convergence (23.2mm) of the site construction method. This result shows that the stress release degree of the surrounding rock of methods 1–3 is considerably higher than that of the site construction method, which is the main reason why the lining stresses of methods 1–3 are lower than that of the site construction method. However, although the stress release of the surrounding rock is beneficial to the supporting structure to some extent, careful monitoring on the displacement of surrounding rock should be conducted to prevent the failure of the surrounding rock due to excessive displacement.

In summary, the stress release degree of surrounding rock of the methods 1–3 is higher than that of the site construction method, which reduces the lining stress but enlarges the rock displacement. Therefore, for cases with small limitations on rock displacement, such as mountain tunnels, method 1–3 is feasible, and method 3 is optimal. However, for urban tunnels or tunnels close to important building structures, the feasibility of these three optimization methods needs further research.

6.2 Construction Optimization in Grade III Rock Mass

In grade III rock mass, the stress distribution of primary support under the site construction method and methods 4–6 is displayed in Fig. 16. Consistent with the lining stress in grade V rock mass, the stress distributions of the four methods are relatively similar, and the lining stress are concentrated in the side wall. Compared with the site construction method, the lining stresses of methods 4–6 are considerably smaller. The maximum lining stresses in the site construction method and methods 4–6 are 8.49 MPa, 7.53 MPa, 7.20 MPa and 6.36 MPa. However, in methods 4–6, the lining stress in the tunnel arch is very small, and even tensile stress (0.2–0.4 MPa) appeared, which is extremely unfavorable since the arch lining is prone to bending failure in this case.

The distribution of rock displacement of the site construction method in grade III rock mass is illustrated in Fig. 17. Similarly, the rock displacement distributions of methods 4–6 are not exhibited. The maximum rock subsidence occurs in the tunnel vault (i.e., point A), and the largest horizontal displacement is concentrated in the wall waist (i.e., points E and K). The magnitudes of the rock
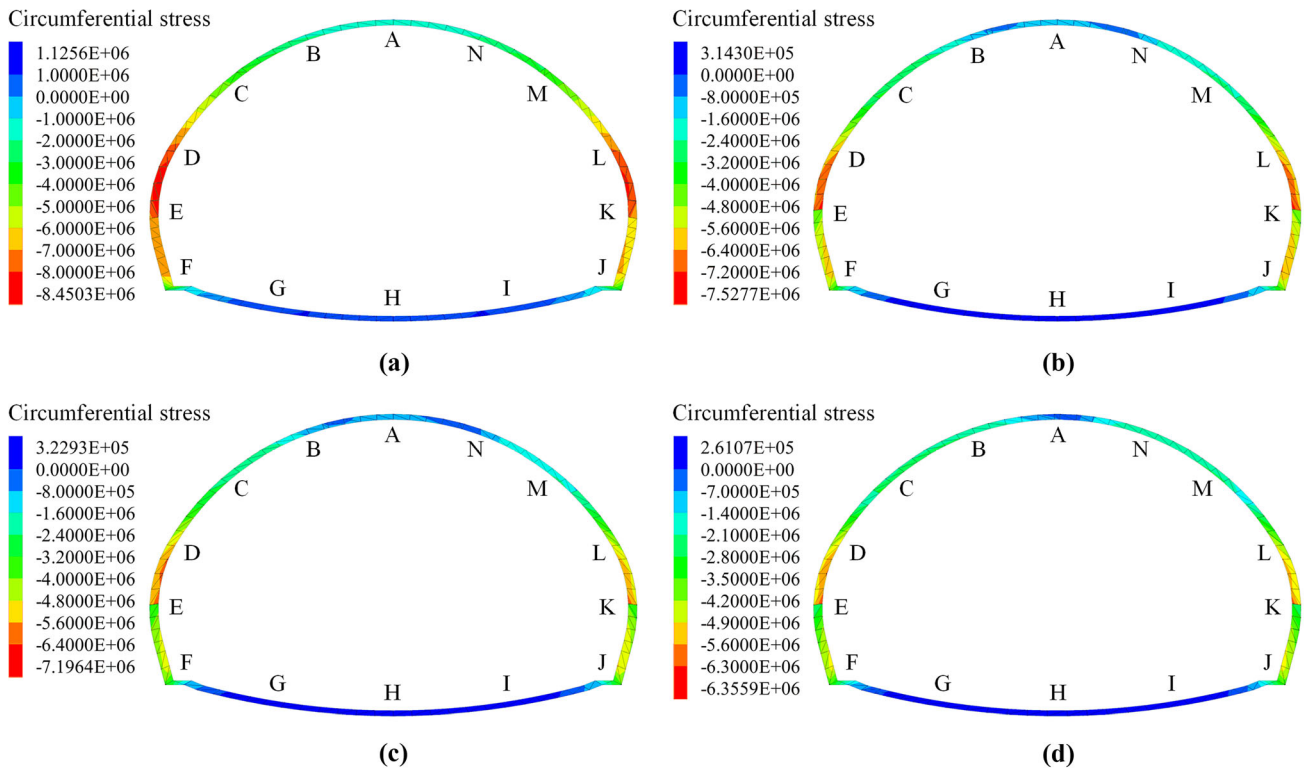
Fig. 16 Lining stress distribution of the site construction method and method 4–6 in grade III rock mass (unit: Pa): **a** site construction method, **b** method 4, **c** method 5, **d** method 6
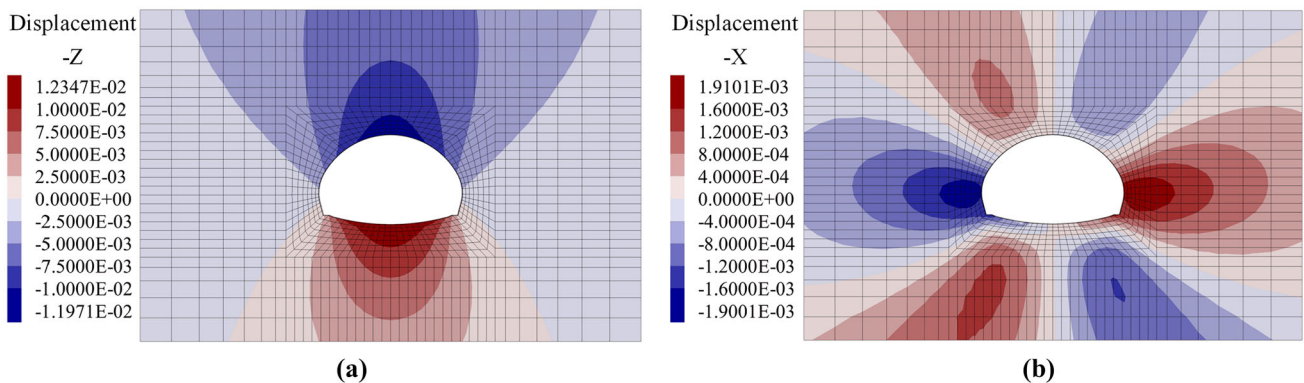

Fig. 17 Rock displacement distribution of the site construction method in grade III rock mass (unit: m): **a** vertical settlement, **b** horizontal convergence

displacements of the four methods are extremely close. The maximum vault settlements of the site construction method and methods 4–6 are 12.0 mm, 13.2 mm, 13.3 mm and 14.6 mm, respectively, and the maximum horizontal convergences are 3.8 mm, 3.9 mm, 4.0 mm and 4.2 mm, respectively. These results imply that the construction method has little influence on the rock displacement of shallow SLS tunnel in grade III rock mass.

To sum up, in grade III rock mass, when the three-step method (methods 4–6) is used to replace the site construction method, the lining stress decreased considerably while the rock displacement remains almost unchanged. Considering the compressive bearing capacity of primary support and the stability of surrounding rock, methods 4–6 are feasible, and method 6 is the best. However, due to the low lining stress at the tunnel arch in methods 4–6, the bending bearing capacity of the primary support in tunnel arch is relatively poor. Therefore, when using the three-step method to construct the shallow SLS tunnels in grade III rock mass, measures such as improving the strength grade and distribution density of steel arches, and increasing the number of circumferential connecting bars
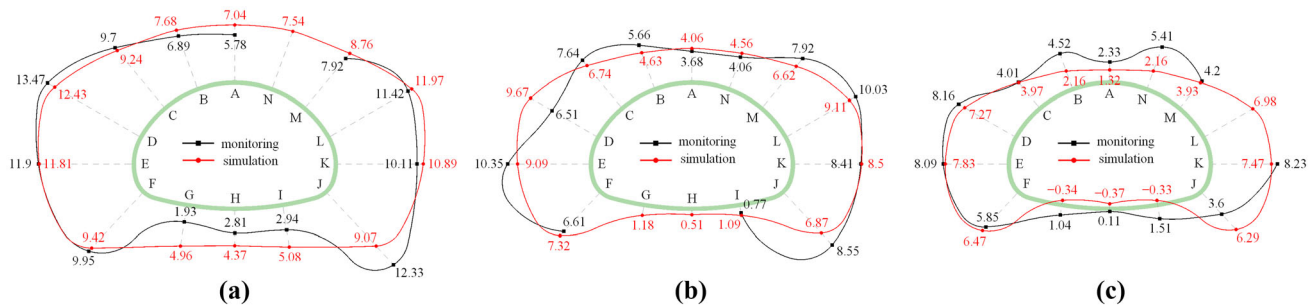
Fig. 18 Comparison between the measured and calculated lining stress (unit: MPa): **a** Sect. 1 (grade V rock mass), **b** Sect. 2 (grade IV rock mass), **c** Sect. 3 (grade III rock mass)

in tunnel arch should be taken to enhance the bending strength of the primary support and prevent it the from bending failure.

6.3 Comparison Between Field Tests and Simulation

As shown in Fig. 18, the distributions of the measured and simulated lining stresses are relatively similar: the shotcrete stress in side wall is significantly greater than that in the tunnel arch and inverted arch, showing a distribution mode of "large in side wall, small in arch and inverted arch." Besides, the magnitude of the measured and simulated lining stresses is also very close. The average lining stresses of Sects. 1 , 2, 3 in field monitoring are 8.24 MPa, 6.68 MPa and 4.39 MPa, respectively, while those in the numerical simulation are 8.59 MPa, 5.71 MPa and 4.06 MPa, respectively. The relative errors of monitoring and simulating lining stress at the three sections are 4.2%, 14.5% and 7.5%, respectively. As a result, it can be confirmed that the simulation results are relatively reliable.

7 Conclusions

Based on the Xiabeishan No. 2 tunnel project in China, the mechanical behavior of surrounding rock and supporting structure of shallow super-large span (SLS) tunnels in grades III–V tuff stratum were comprehensively investigated by field monitoring. Then, combined with finite difference program and laboratory test, the fine numerical simulation of excavation and support of Xiabeishan No. 2 tunnel is realized, and the lining stress and surrounding rock displacement of each optimized construction scheme are comprehensively compared and analyzed. The conclusions are as follows:

(1) The excavation disturbance created by the construction of shallow SLS tunnel is mainly concentrated on the upper benches. The construction of the upper bench of the middle heading, in which the super-large span structure is formed, is the most critical construction step. The construction management and monitoring should be strictly strengthened in these construction stages to reduce the construction risks.

(2) The blasting vibration created by the construction of the middle heading caused serious damage to the temporary support, and the stress adjustment of the rock mass and supporting structures was completed before the demolition of temporary support, which caused great construction risks. The accuracy of drilling and charging should be strictly guaranteed, and the thickness and reinforcement ratio of temporary support should be appropriately increased in the construction of shallow SLS tunnels.

(3) The distribution of rock pressure and lining stress in grades VI–V rock mass is similar to those in grade III rock mass. The surrounding rock pressure shows a distribution pattern of "large in upper bench, small in lower bench," while the lining stress shows the characteristics of "large in side wall, small in arch and inverted arch." However, the magnitude of rock pressure and lining stress in grade V rock mass are approximately 2–3 times that in grade III rock mass.

(4) For shallow SLS tunnels with limitations on rock displacement, the "middle first and side later" double side heading method in grades IV–V rock mass is feasible. When the three-step method is adopted in grade III rock mass, measures such as improving the strength grade and distribution density of steel arches, and increasing the number of circumferential connecting bars in tunnel arch should be taken to and prevent the primary support from bending failure.

Springer

manuscript. No conflict of interest exits in the submission of the manuscript.

Data availability The data presented in this article are available on request from the corresponding author.

Declarations

Conflict of interest The authors declare that they have no known competing financial interests or personal relationships that could have appeared to influence the work reported in this paper.

References

1. Tonon F (2011) ADECO full-face tunnel excavation of two 260 m(2) tubes in clays with sub-horizontal jet-grouting under minimal urban cover. Tunn Undergr Space Technol 26(2):253–266. https://doi.org/10.1016/j.tust.2010.09.006

2. Zhang TZ (2015) Analysis of mechanical response of four-lane small clear spacing highway tunnel with super-large cross-section. Chin Civil Eng J 48(s1):302–305

3. Gong YF, Zhang JR, Xu XD et al (2015) Design technology for super large cross section tunnel in stratum of completely weathered granite with abundant water. J Railway Eng Soc 32(10):79–85

4. Gao HB (2010) Study on mechanical performance for the construction of a large-span Railway Station tunnel. Mod Tunn Technol 47(3):32–38. https://doi.org/10.13807/j.cnki.mtt.2010.03.006

5. Ding JL (2005) Reasonable method for the construction of shallow-depth and wide-span tunnel. China Railway Sci 26(4):77–81

6. Tu HL, Zhou H, Qiao CS et al (2020) Excavation and kinematic analysis of a shallow large-span tunnel in an up-soft/low-hard rock stratum. Tunn Undergr Space Technol 97:103245. https://doi.org/10.1016/j.tust.2019.103245

7. Wu MJ, Huang LH (2006) Research on dynamic construction mechanics of four-lane highway tunnel. Chin J Rock Mech Eng 25(S1):3057–3062

8. Zhao B, Zhang HJ, Qiu WG (2014) A study of stress evolution during construction of extra-large cross section railway tunnels. Mod Tunn Technol 51(1):70–76. https://doi.org/10.13807/j.cnki.mtt.2014.01.013

9. Luo YB, Chen JX, Shi Z et al (2020) Mechanical and deformation characteristics and optimization of support parameters for superlarge-span tunnel: a case study from Laohushan tunnel. Adv Civil Eng 2020:8882019. https://doi.org/10.1155/2020/8882019

10. Li B, Song Y, Shi YL et al (2015) Study on mechanical and deformation characteristics of large cross-section loess tunnels constructed by different methods. Tunn Constr 35(6):508–513. https://doi.org/10.3973/j.issn.1672-741X.2015.06.003

11. Luo YB, Chen JX, Shi Z et al (2020) Mechanical characteristics of primary support of large span loess highway tunnel: a case study in Shaanxi Province, Loess Plateau, NW China primary. Tunn Undergr Space Technol 104:103532. https://doi.org/10.1016/j.tust.2020.103532

12. Qi H, Shang CS, Hu C et al (2020) Study on stability of rock supporting structure during construction of super-large cross-section tunnel. Yangtze River 51(9):135–141. https://doi.org/10.16232/j.cnki.1001-4179.2020.09.024

13. Luo YB, Chen JX, Shi Z et al (2020) Performance of super-large-span tunnel portal excavated by upper bench cd method based on field monitoring and numerical modeling. Adv Civil Eng 2020:8824618. https://doi.org/10.1155/2020/8824618

14. Zhou DH, Cao LQ, Ma YF et al (2010) Research on construction behaviors of support system in four-lane ultra large-span tunnel with super-large cross-section. Chin J Rock Mech Eng 29(1):140–148

15. Chen JX, Xu ZL, Luo YB et al (2020) Application of the upper-bench CD method in super large-span and shallow tunnel: a case study of letuan tunnel. Adv Civil Eng 2020:8826232. https://doi.org/10.1155/2020/8826232

16. Chen GY, Liu B, Wan MF et al (2005) Analysis of stress monitoring of a large-span highway tunnel in Hanjialing mountain. Chin J Rock Mech Eng 24(S2):5509–5515

17. Liu QS, Peng XX, Lei GF et al (2017) Geomechanical model test on excavation technology of supper-large cross-section ultra-shallow tunnel with cross rock pillar method. Rock Soil Mech 38(10):2780–2788. https://doi.org/10.16285/j.rsm.2017.10.002

18. Wu QK (2019) Study on construction technology and stability of ultra-shallow buried extra large section of Wulidian Station. Dissertation, Anhui University of Science and Technology

19. Qing WC, Gao Y, Zhu Y et al (2018) Construction methods for ultra large-span four-track deep tunnel on Wumengshan No. 2 exit section. Tunn Constr 38(1):91–102. https://doi.org/10.3973/j.issn.2096-4498.2018.01.012

20. Hong J, Zhang JR (2016) Analysis of support stress of extra-large cross-section tunnel during construction in fully weathered granite strata. Tunn Constr 36(7):787–792. https://doi.org/10.3973/j.issn.1672-741X.2016.07.003

21. Wang DB (2016) Construction technology for separated and combined excavation section of phoenix mountain tunnel with composite double side heading method. Mod Tunn Technol 53(S2):634–638. https://doi.org/10.13807/j.cnki.mtt.2016.2.094

22. The Professional Standards Compilation Group of People's Republic of China (2015) Technical specification for monitoring measurement of railway tunnel (Q/CR 9218–2015). China Railway Publishing House, Beijing

23. Lazemi HA, Marji MF, Bafghi ARY et al (2013) Rock failure analysis of the broken zone around a circular opening. Arch Min Sci 58(1):165–188. https://doi.org/10.2478/amsc-2013-0012

24. Nikadat N, Fatehi M, Abdollahipour A (2015) Numerical modelling of stress analysis around rectangular tunnels with large discontinuities (fault) by a hybridized indirect BEM. J Central South Univ 22(11):4291–4299. https://doi.org/10.1007/s11771-015-2977-9

25. Abdollahi MS, Najafi M, Bafghi AY et al (2019) A 3D numerical model to determine suitable reinforcement strategies for passing TBM through a fault zone, a case study: Safaroud water transmission tunnel, Iran. Tunn Undergr Space Technol 88:186–199. https://doi.org/10.1016/j.tust.2019.03.008

26. Fenner R (1938) Untersuchungen zur erkenntnis des gebirgsdrucks. Glückauf 74:681–715

27. Vitali OPM, Celestino TB, Bobet A (2018) 3D finite element modelling optimization for deep tunnels with material nonlinearity. Undergr Space 3(2):125–139. https://doi.org/10.1016/j.undsp.2017.11.002

28. Xiao Y, He M, Qiao Y et al (2023) A novel semi-analytical solution to ground reactions of deeply buried tunnels considering the nonlinear behavior of rocks. Comput Geotech 159:105429. https://doi.org/10.1016/j.compgeo.2023.105429

29. Lee Y-K, Pietruszczak S (2008) A new numerical procedure for elasto-plastic analysis of a circular opening excavated in a strain-softening rock mass. Tunn Undergr Space Technol 23(5):588–599. https://doi.org/10.1016/j.tust.2007.11.002

30. He JX, He SH, Liu XB et al (2022) Structural design and mechanical responses of closely spaced super-span double

tunnels in strongly weathered tuff strata. Front Struct Civ Eng 16(6):685–703. https://doi.org/10.1007/s11709-022-0824-2

31. Ministry of Housing and Urban-Rural Development of the People's Republic of China (2013) Standard for test methods of engineering rock mass (GB/T 50266–2013). China planning press, Beijing

32. Sonmez H, Ulusay R (1999) Modifications to the geological strength index (GSI) and their applicability to stability of slopes. Int J Rock Mech Min Sci 36(6):743–760. https://doi.org/10.1016/s0148-9062(99)00043-1

33. Hoek E, Brown ET (1997) Practical estimates of rock mass strength. Int J Rock Mech Min Sci 34(8):1165–1186. https://doi.org/10.1016/s1365-1609(97)80069-x

34. Cai M, Kaiser PK, Uno H et al (2004) Estimation of rock mass deformation modulus and strength of jointed hard rock masses using the GSI system. Int J Rock Mech Min Sci 41(1):3–19. https://doi.org/10.1016/s1365-1609(03)00025-x

35. Luo YB, Shi Z, Chen JX et al (2020) Mechanical calculation model and research on construction mechanical behavior of middle diaphragm in upper bench CD method for super-large span tunnel. China J Highw Transp 33(12):235–248. https://doi.org/10.19721/j.cnki.1001-7372.2020.12.019

36. Zhang HJ, Wang ZZ, Lu F et al (2018) Analysis of the displacement increment induced by removing temporary linings and corresponding countermeasures. Tunn Undergr Space Technol 73:236–243. https://doi.org/10.1016/j.tust.2017.12.025

37. Yuan Y, Wang SH (2008) Numerical modeling of pre-built and prestressed innovative support system for super cross-section highway tunnel with lower flat-ratio. Rock Soil Mech 29(1):240–244

38. Qu WB (2009) Construction mechanics effect of pile-beam-arch tunneling method in metro construction. Dissertation, Chongqing University

39. Li R, Zhang DL, Fang Q et al (2020) Mechanical responses of closely spaced large span triple tunnels. Tunn Undergr Space Technol 105:103574. https://doi.org/10.1016/j.tust.2020.103574

40. State Railway Administration of the People's Republic of China (2016) Code for design of railway tunnel (TB 10003–2016). China Railway Publishing House, Beijing

41. Wu MF (2010) Study on primary support method for large section railway station tunnel with four-track. Dissertation, Southwest Jiaotong University

42. Liu DP, Zhang DL, Fang Q et al (2020) Field monitoring of the deformation and internal forces of the surrounding rock and support structures in the construction of a super-span high-speed railway tunnel-A case study. Appl Sci Basel 10(15):5182. https://doi.org/10.3390/app10155182